Applied Physics Letters

RESEARCH ARTICLE | OCTOBER 08 2024

Steering sound propagation with Zeno barriers in acoustic waveguide arrays

Ze-Xin Huang ; Hong-Wei Wu ; Le-Le Cheng; Peng-Xiang Xie ; Xue Chen ; Hua-Feng Xu; Zong-Qiang Sheng

Appl. Phys. Lett. 125, 152201 (2024)
https://doi.org/10.1063/5.0234559

AIP Publishing

Applied Physics Letters ARTICLE pubs.aip.org/aip/apl

Steering sound propagation with Zeno barriers in acoustic waveguide arrays

Cite as: Appl. Phys. Lett. **125**, 152201 (2024); doi: 10.1063/5.0234559
Submitted: 22 August 2024 · Accepted: 29 September 2024 ·
Published Online: 8 October 2024

View Online Export Citation CrossMark

Ze-Xin Huang,[1] Hong-Wei Wu,[1,2,3,a)] Le-Le Cheng,[1] Peng-Xiang Xie,[1] Xue Chen,[1,2] Hua-Feng Xu,[1,2] and Zong-Qiang Sheng[1,2]

AFFILIATIONS

[1]School of Mechanics and Photoelectric Physics, Anhui University of Science and Technology, Huainan 232001, China
[2]Center for Fundamental Physics, Anhui University of Science and Technology, Huainan 232001, China
[3]Institute of Energy, Hefei Comprehensive National Science Center (Anhui Energy Laboratory), Hefei 230031, China

[a)]Author to whom correspondence should be addressed: hwwu@aust.edu.cn

ABSTRACT

In quantum systems, a counterintuitive phenomenon known as quantum Zeno dynamics is usually exploited to tailor and protect the coherent evolution of quantum states by the back action of quantum measurements and strong couplings. Here, with the quantum-classical analogy, we report that the acoustic Zeno dynamics can be reproduced in acoustic waveguide arrays by setting segmented waveguides. We experimentally demonstrate that the segmented waveguide acts as an acoustic barrier to tailor the whole Hilbert space into different subspaces by separating the communication between waveguides. By arranging the acoustic Zeno barriers, we can control the sound transport in waveguide arrays into the target output ports, such as the Zeno dynamics, analog-quantum walk, and analog-quantum logic gates. In this context, we highlight that the Zeno barrier can be a versatile tool to arbitrarily control and guide the sound transport in waveguide arrays, which can provide an alternative choice for acoustic metamaterials and metasurfaces without cumbersome and complicated structure design. The acoustic Zeno barrier may provide a versatile approach to manipulate acoustic wave propagation for designing advanced on-chip integrated sound devices.

Manipulating physical fields to satisfy various advanced applications is an immutable subject in different physical branches. For example, in classical sound wave systems, the concept of acoustic metamaterials and metasurfaces designed with subwavelength structure units have been proposed to manipulate the wave propagation, such as wave focusing,[1–6] extraordinary transmission,[7–9] and acoustic insulators.[10–12] The quantum system always has unique characteristics that are different from classical waves. With the development of a quantum-classic analogy, many quantum effects have been explored in classical systems. A prominent example is the topological insulators[13–18] that possess robust topological protected properties for manipulating the wave propagation against the disorder and defects, which have grown into a large research field in photonic and phononic crystals. Furthermore, emulating the electrons in semiconductors, phononic lattices have provided a versatile platform for manipulating acoustic waves based on the similar formation between the Schrödinger equation for matter waves and the paraxial Helmholtz equation for acoustic waves. In this context, the temporal evolution of a quantum system corresponds to the spatial sound propagation in waveguide arrays, and many similar quantum phenomena have been realized in acoustic waves, such as Bloch oscillations,[19,20] Landau–Zener transition,[21] and Anderson localization,[22,23] among others.[24,25] Furthermore, stimulated Raman adiabatic passage is also proposed in acoustics to achieve selective and efficient population transfer between two quantum states by designing the time-dependent coupling mediated intermediate state without suffering loss for manipulating sound transports.[26–31]

The quantum Zeno effect is a counterintuitive phenomenon in an unstable quantum state that inhibits coherent evolution to another state under frequent observation. From the decay view of the quantum state, it is well known that the survival probability P is quadratic at short times, i.e., $dP/dt \rightarrow 0$ for $t \rightarrow 0$.[32] The Zeno effect has been experimentally confirmed in a variety of physical systems, such as trapping atoms,[33] Bose–Einstein condensates,[34] cavity quantum electrodynamics,[35,36] Rydberg atoms,[37] and optical waveguide arrays.[38] More interestingly, the quantum Zeno dynamics have also been experimentally demonstrated, showing that the back action of quantum measurements can be explored to preserve a coherent evolution in a subspace of the Hilbert space by engineering the Zeno dynamic boundaries in the Bose–Einstein condensate system.[34] Recently, in optical systems, tailoring Hilbert space has been explored as an approach for controlling and manipulating the evolution of the optical system.[39] However, Zeno dynamics had not been realized in acoustic systems until now. Traditional sound wave manipulation typically involves designing anisotropic and inhomogeneous acoustic metamaterials to guide wave propagation. In contrast, Zeno dynamics could be a powerful tool for designing acoustic evolution subspaces. By flexibly placing Zeno barriers in space, it is possible to control sound wave propagation paths, enabling various advanced acoustic applications and offering an alternative approach to acoustic metamaterials.

In this paper, we experimentally demonstrate the Zeno dynamics in an acoustic waveguide array system. A Zeno barrier is constructed by segmented waveguides to tailor the Hilbert space of a five-waveguide system into different subspaces. The result indicates that frequent measurement of the third waveguide can transfer the free evolved acoustic field into two Hilbert subspaces to form a Rabi oscillation. Using the acoustic Zeno barriers as a versatile tool, we can arbitrarily control and guide the sound transport in waveguide arrays into the target output ports for engineering different advanced functions, such as the Zeno dynamic, analog-quantum walk, and analog-quantum logic gates. By shortening the structure and increasing the incident frequency, the acoustic Zeno barrier can provide a versatile tool for controlling sound wave propagation in the design of advanced on-chip integrated acoustic devices, with applications in areas such as acoustic cloaking and sound insulation.

Without loss of generality, we first consider a model of five-level quantum system with state transitions $|1\rangle \longleftrightarrow \cdots \longleftrightarrow |5\rangle$ with coupling strength κ; then a detector denoted by $|D\rangle$ is used to frequently measure the third level with a coupling strength c as shown in Fig. 1(a). To describe the dynamic evolution, the Hamiltonian of five-level quantum system with frequent measurements can be expressed as[40,41]

$$H = \sum_{i=1}^{5} \kappa(|i\rangle\langle i+1| + |i+1\rangle\langle i|) + c(|3\rangle\langle D| + |D\rangle\langle 3|) - i\Gamma|D\rangle\langle D|, \quad (1)$$

where κ corresponds to the coupling strength between these five levels, c is the coupling strength between the detector D with dissipation Γ and the third level $|3\rangle$. If $c \gg \kappa$, then the total Hilbert space is divided into four subspaces: $\oplus$ subspace 1 (levels $|1\rangle$ and $|2\rangle$), $\oplus$ subspace 2 (levels $|4\rangle$ and $|5\rangle$), $\oplus$ subspace 3 (level $|3\rangle + |D\rangle$), $\oplus$ subspace 4 (level $|3\rangle - |D\rangle$). Notice that the Rabi oscillations will be restored in subspace 1 and subspace 2. Similar research works for tailoring the Hilbert space have been discussed in quantum system,[40] Bose–Einstein condensates,[34] and classical optical system.[39] "A watched cook can freely watch a boiling pot."

Here, we construct the frequently measured Hilbert space by designing acoustic waveguides in an acoustic system as shown in Fig. 1(b), the spoof surface acoustic waves (SSAWs) propagating and evanescent coupling between the five green straight waveguides for simulating the five-level quantum system. Here, we select the SSAWs to investigate the acoustic Zeno effect due to the propagation constants and coupling freely tunable by adjusting the waveguide parameters.

The green acoustic waveguides are constructed by placing a series of rigid sheets with a spacing $a = 18$ mm between the sheets and a period $\Lambda = a + b = 20$ mm, where b is the thickness of the small sheet, the sheet width is set as $W_1 = 30$ mm and the interval between waveguides as $d_1 = 70$ mm. To introduce the frequent measurement, we place a red segmented waveguide acting as a frequent observation to form the Zeno barrier (ZB) and couple it with waveguide 3 (WG3) of

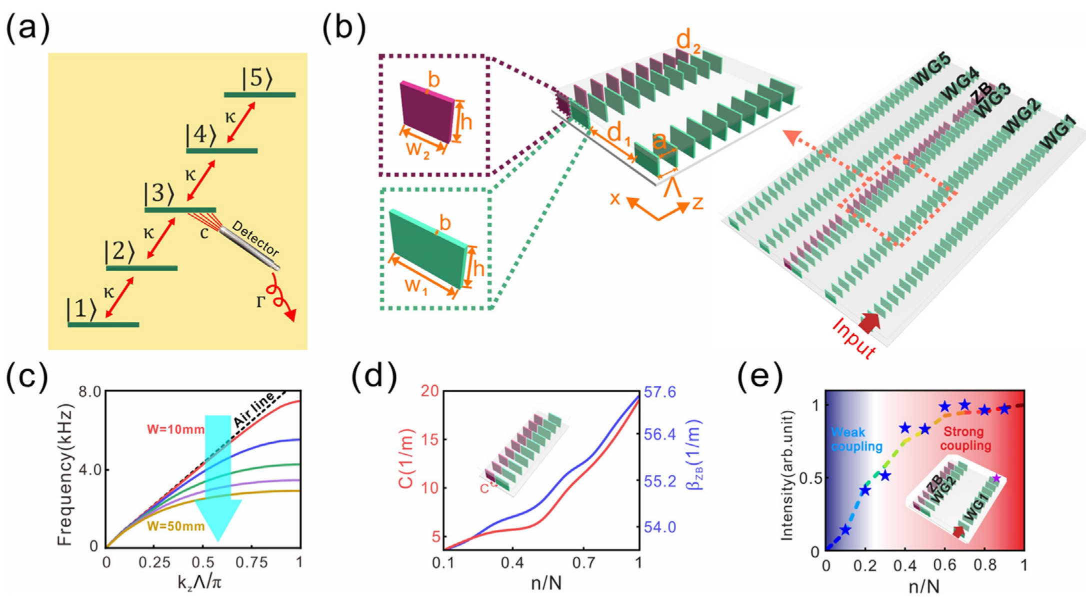

FIG. 1. (a) Schematic diagram of a five-level quantum system. The Hilbert space is tailored by frequent measurements of a detector for level |3. (b) Schematic diagram of acoustic waveguide array. (c) Dispersion relation for different waveguide widths. (d) Under different observation frequencies, the coupling coefficient c (red line) between the observed waveguide and the third waveguide and the propagation constant β_{ZB} (blue line) of the observed waveguide. (e) The intensity of acoustic pressure on the incident waveguide at different measured frequencies. The dashed lines are simulation results, and the blue stars are experimental measurements.

the five-level system at a distance $d_2 = 2.5$ mm to achieve strong coupling. A sound with $f_{in} = 2950$ Hz is inputted from waveguide 1 (WG1). The segmented waveguide is constructed by small sheets with width $W_2 = 20$ mm. The whole waveguide arrays are sandwiched by two rigid plates as a two-dimensional (2D) scenario. The waveguide dispersive relationship for different sheet widths is shown in Fig. 1(c) according to the expression $k_z = k_0\sqrt{1 + \left[\frac{a}{\Lambda}/\tan\left(\frac{k_0 W+\pi}{2}\right)\right]^2}$.[42] We can find that the SSAWs with lower cutoff frequency will be supported along the waveguide for wider sheets. The SSAW will be more confined with weaker coupling between adjacent waveguides for the working frequency near to the cutoff frequency. To simulate the frequent observation, we define the observing frequency as $f_{\rm obs} = n/N$, where $N = 10$ is the total number of sheets in an observed distance $l = 10\Lambda$ for an incident frequency $f_{in} = 2950$ Hz; then $f_{\rm obs} = 0$ and 1 represent no observation and continuous observation. To clarify the coupling strength between the observing waveguide and the third waveguide for different observed frequencies, we calculate the coupling coefficient c as the function of n/N by extracting the transferring length in the two-waveguide system as shown in the inset of Fig. 1(d). The detail of the method is illustrated in Sec. I of the supplementary material. The results indicate that the coupling coefficient c and the propagation constant β_{ZB} of the segmented waveguide increase with increasing observing frequency shown as the red line and blue line, respectively.

To further evaluate the influence of observing frequency $f_{\rm obs}$ on the acoustic field evolution, we also calculate and measure the acoustic intensity $I = |\psi(0)|\psi(z)|^2$ for $z \in [0, L/2]$ in frequently observed two-waveguide system as shown in Fig. 1(e) for different $f_{\rm obs}$. Here, $L = 2.2$ m corresponds to the whole Rabi oscillated length, in which $L = 11l$. The red arrow and pentalpha in the inset represent the incident and receiving locations. The dashed line is obtained from the finite-element simulation using the commercial software COMSOL Multiphysics, and the symbols correspond to the experimental results. The simulated and measured details, as well as the normalized processing for the measured pressure fields, are presented in the supplementary material. We can find that the acoustic field freely hops between two waveguides for $f_{\rm obs} = 0$, which corresponds to the Rabi oscillation of the two-level model, then $I = 0$. However, the field hop becomes inhomogeneous between the WG1 and WG2 as the observing frequency increases. When the observing frequency reaches $f_{\rm obs} = 1$, the acoustic field is frozen in the incident waveguide, resulting in $I = 1$, which corresponds to the Zeno effect. In Fig. 1(e), we can find that the sound intensity mainly resides in the incident waveguide for the observing frequency over $f_{\rm obs} = 0.3$. In other word, the coupling strength between the ZB and WG2 go into the strong coupling region for $f_{\rm obs} > 0.3$. To obtain excellent performance, we select the observing frequency $f_{\rm obs} = 0.9$ in the following investigations. The defect of a sheet for forming the dissipative simulate the role of Γ in quantum system.

Assuming weak coupling between the five straight waveguides, we arrive at the tight-binding-approximated (TBA) Schrödinger-type equation for the observed five-waveguide system, considering only nearest-neighbor couplings as

$$i\frac{d\psi(z)}{dz} = H\psi(z), \quad (2)$$

where the acoustic field envelope is $\psi(z) = [\psi_1(z), \ldots, \psi_5(z), \psi_{ZB}(z)]^T$, and the initial state is $\psi(0) = [1, 0, 0, 0, 0, 0]^T$ for inputting from WG1, as shown in Fig. 1(b). Using the ZB to observe WG3, the coupling between the green straight waveguides is κ, with propagation constants $\beta_{WG1} = \cdots = \beta_{WG5} = \beta$. The coupling between the red segmented waveguide and the green straight waveguides is c, and the propagation constant of the segmented waveguide is β_{ZB}. $\Gamma = 0.1c$ is the dissipation due to the observed frequency $f_{\rm obs} = 0.9$. The Hamiltonian can be expressed as follows:[34,39,43]

$$H = \begin{bmatrix} \beta_{WG1} & \kappa & 0 & 0 & 0 & 0 \\ \kappa & \beta_{WG2} & \kappa & 0 & 0 & 0 \\ 0 & \kappa & \beta_{WG3} & \kappa & 0 & c \\ 0 & 0 & \kappa & \beta_{WG4} & \kappa & 0 \\ 0 & 0 & 0 & \kappa & \beta_{WG5} & 0 \\ 0 & 0 & c & 0 & 0 & (\beta_{ZB} - i\Gamma) \end{bmatrix}. \quad (3)$$

Figure 2(a) shows the acoustic field evolution in five-waveguide system without frequent observation, and we can find that the acoustic field freely evolves in the waveguide array by the nearest-neighbor coupling by solving Eq. (2). The simulated result is also presented in Fig. 2(d), which agree well with the theoretical result. Here, we only show the first oscillation from WG1 to WG5 in the waveguide length $L = 2.2$ m. When we introduce the observed segmented waveguide to couple strongly with the third waveguide, the whole Hilbert space splits into four subspaces: subspace 1 (levels $|1\rangle$ and $|2\rangle$) $\oplus$ subspace 2 (levels $|4\rangle$ and $|5\rangle$) $\oplus$ subspace 3 (level $|3\rangle + |ZB\rangle$) $\oplus$ subspace 4 (level $|3\rangle - |ZB\rangle$). Here, $|ZB\rangle$ corresponds to the Zeno barrier constructed by the segmented waveguide. In the language of quantum Zeno dynamics,[40] the Hamiltonian of the closed five-waveguide system is given by $H_c = \kappa(|1\rangle\langle 2| + |2\rangle\langle 3| + |3\rangle\langle 4| + |4\rangle\langle 5| + H.c.)$. Then the ZB coupling with WG3 corresponds to a projector as $P_3 = \boldsymbol{I} - |3\rangle\langle 3|$; thus, the effective Hamiltonian can be obtained by $H_P = P_i H_c P_i$ as $H_P = \kappa(|1\rangle\langle 2| + |4\rangle\langle 5| + H.c.)$, where subscript i correspond to the ith observed waveguide. That is to say, WG3 forms a hard wall to inhibit the communication between the subspaces: subspace 1 (levels $|1\rangle$ and $|2\rangle$) $\oplus$ subspace 2 (levels $|4\rangle$ and $|5\rangle$), and then the input acoustic field hops between WG1 and WG2 or WG4 and WG5 to form the Rabi oscillations, which have been demonstrated by theoretical calculation and numerical simulation as shown in Figs. 2(b)–2(f), accordingly.

We have demonstrated that a Zeno barrier can be constructed using a segmented waveguide to tailor the acoustic Hilbert space for guiding sound evolution in a waveguide array. Next, to further demonstrate how the Zeno barrier can be used to manipulate sound for practical applications in waveguide arrays. Figure 3(a) shows the sample for controlling the sound transport into different target ports as a quantum walk. The whole system includes five waveguides, and the sound is injected into the first waveguide. There are two rows of insertable grooves for each waveguide; when inserting sheets into the grooves, the segmented waveguides ($n/N = 0.9$) will be formed as a Zeno barrier to tailor the coupling of waveguides, as shown as Fig. 1(b). The whole 2D sample includes four sections, and the length of every section is $L/2$, which corresponds to half the period of Rabi oscillation. For the clarity of presentation, we only show two sections in Fig. 3(a).

Now, we construct the Zeno barriers in different sections by inserting segmented waveguides for ring-fencing the sound evolution. In Fig. 3(b), we show the segmented waveguide distribution as ZB P_2

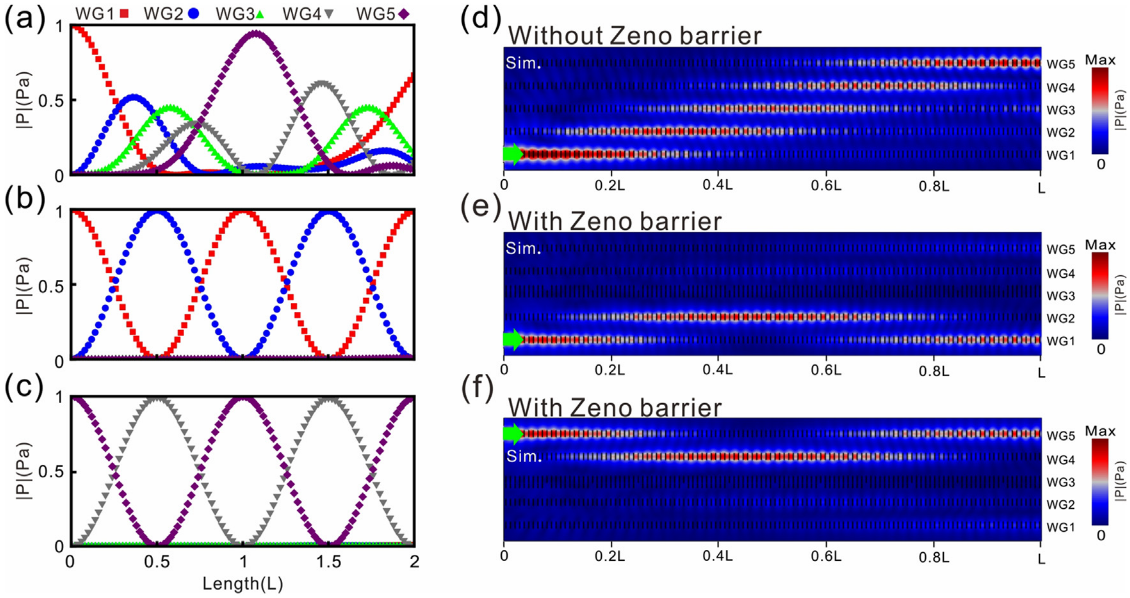

FIG. 2. (a) Evolution of acoustic field in a five-waveguide system without frequent observations. (b) and (c) When the third waveguide is observed frequently, the acoustic field evolution of the five-waveguide system when the acoustic is incident from WG1 (b) and WG5 (c), respectively. (d)–(f) Corresponding to the simulation results of figure (a), (b), and (c), respectively.

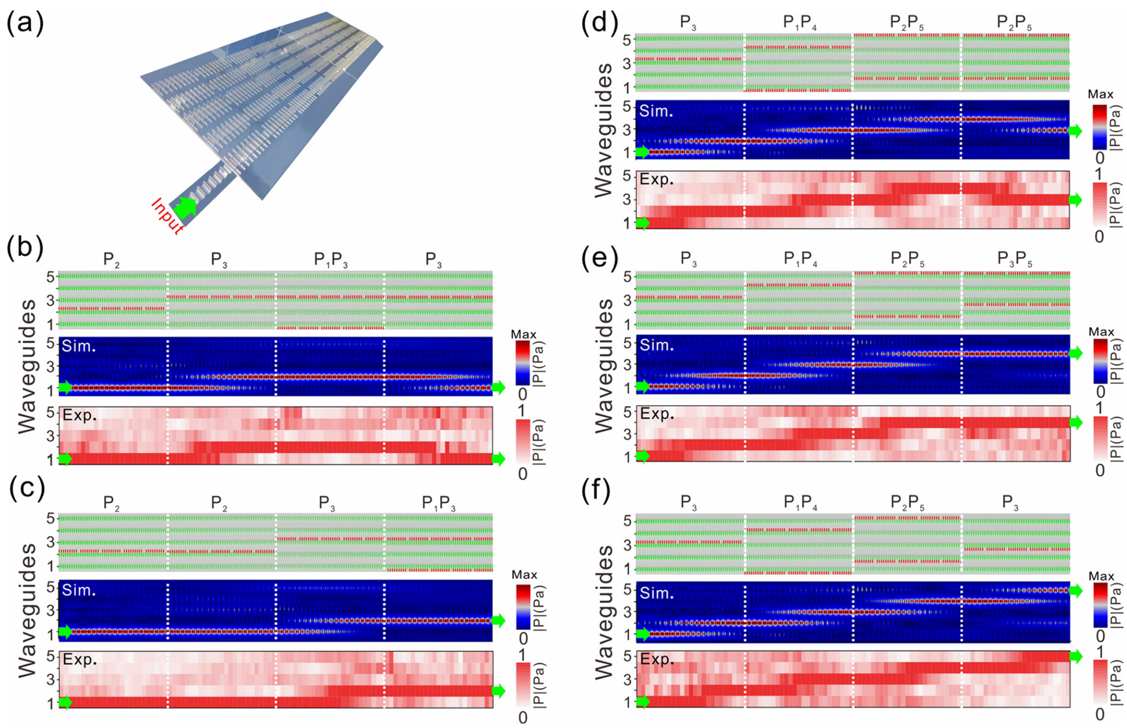

FIG. 3. (a) The experiment sample. The total length of the waveguide is 4m, and only 2 m is displayed for clarity. The waveguide array consists of five waveguides. The segmented waveguide can be inserted into grooves on both sides of the straight waveguide as ring fencing. (b)–(f) Waveguide diagram, simulation calculation, and experimental measurement of the acoustic wave guided to different output ports.

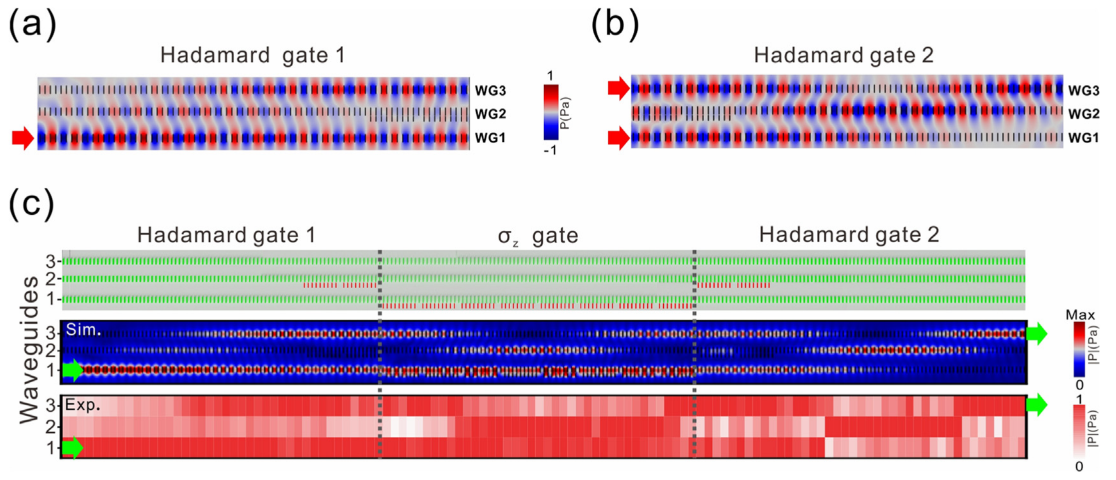

FIG. 4. (a) Acoustic pressure simulation of Hadamard gate 1 for inputting from WG1. (b) Acoustic pressure simulation of Hadamard gate 2 for inputting from WG1 and WG3. (c) The X gate is implemented by adding Z gate between Hadamard gate 1 and Hadamard gate 2, and the sound input from WG1 to output port WG3.

in section 1, ZB P_3 in section 2, ZB P_1 and P_3 in section 3, and ZB P_3 in section 4 to guide the sound into the first output port. When the input sound enters the first waveguide, it directly propagates along WG1 due to the existence of ZB P_2, which can be verified by simulation and experiment in section 1. In section 2, the ZB P_3 is used to tailor the whole Hilbert space, as shown in the illustration in Fig. 2. Thus, the sound will couple into WG2 at the end of section 2. In section 3, the ZB are used for WG1 and WG3; the sound will propagate along WG2 only. In the fourth section, the ZB P_3 gives a free evolution subspace to manipulate the sound into output port 1. The whole evolution process, in four sections, can be observed through numerical simulation and experimentation. Similarly, we can also guide the sound walk into different output ports 2, 3, 4, and 5 by setting appropriate ZBs in different sections, as shown in Figs. 3(c)–3(f). The results indicate that the Zeno barrier could be a versatile tool for the control and manipulation of sound transport in the acoustic waveguide array. Based on the strong capacity of the Zeno barrier for ring-fencing the sound evolution, we also add two examples in the supplementary material to demonstrate that the X- and Y-type evolution for two port inputting in acoustic waveguide arrays is controlled by acoustic Zeno barriers. We believe that the Zeno barrier can be explored to realize more advanced acoustic devices based on waveguides by simply placing the ZBs into an acoustic waveguide system.

In the following example, we further realize quantum logical gates: σ_H gate (Hadamard gate), σ_z gate (Z gate), and σ_x gate (X gate) in the acoustic waveguide array by using the Zeno barriers. It is well known that the Hadamard gate satisfies the logical relation:[44] $H|0\rangle = 1/\sqrt{2}(|0\rangle + |1\rangle)$ and $H|1\rangle = 1/\sqrt{2}(|0\rangle - |1\rangle)$, here $|0\rangle = \binom{1}{0}$ and $|1\rangle = \binom{0}{1}$. To realize the Hadamard gate function, we construct the three-waveguide system with the following structure details: the acoustic waveguide length as 1.62 m, the distance $l_1 = 70$ mm between WG1 and WG2, and $l_2 = 52$ mm between WG2 and WG3 for obtaining the coupling constant to split the input field into WG1 and WG3 equally. There are two segmented waveguides presented at the end of WG2 as Zeno barriers to block the hopping between WG1 and WG3 to realize the Hadamard gate. When the input sound with frequency 3175 Hz is injected into WG1, then the state is defined as $|1\rangle = \binom{0}{1}$. By means of a numerical simulation with COMSOL Multiphysics, we can find that the output sound is distributed at WG1 and WG3 with opposite phases, as shown in Fig. 4(a), which is called Hadamard gate 1. However, if we inject the in-phase sound from WG1 and WG3 simultaneously, it is obvious that the sound will be collected into WG3 according to the logical relation of the Hadamard gate in Fig. 4(b), which is called Hadamard gate 2. Here, the two Zeno barriers are placed at the head of WG2. With the above simulations of the Hadamard gates in the three-waveguide system, we know that the X gate (sound injected from WG1 and output from WG3) can be realized by adding a phase π between WG1 and WG3. For this target, we insert a Z gate into the interval of Hadamard gate 1 and Hadamard gate 2 to construct the X gate as shown in Fig. 4(c). The simulated result indicates that WG1 be frozen by the Zeno barrier to cut the communication with WG2 in the Z gate, and the sound injected from WG3 evolves freely between WG3 and WG2. In the waveguide length of 1.62 m, the sound adds a π phase compared with the sound propagating in WG1 and returning to WG3. The experimental measurement verifies the simulated results that the X gate can be realized for transferring sound from WG1 to WG3 by combining the Hadamard gate 1, Z gate, and Hadamard gate 2. Although the waveguide arrays investigated earlier are large, these examples encourage designing advanced on-chip integrated sound devices for various applications in higher working frequency with a small size.

In summary, we experimentally realize the Zeno dynamics in an acoustic waveguide array by using the on-demand periodically segmented waveguides as frequent observation. The results show that a Zeno barrier can be designed to tailor the Hilbert space of the waveguide system into subspaces to control sound evolution. In this content, we also realize acoustic analogies of the quantum walk (the same input end into different output ends) and quantum logical gates (Hadamard gates, Z gate, and X gate) by designing the Zeno barriers in a waveguide array. These practical examples indicate that the Zeno barrier, based on the concept of frequent observation, can provide a versatile tool to tailor and manipulate the sound transport in acoustic waveguides. Undoubtedly, by shortening the structure and increasing the incident frequency, the acoustic Zeno barrier can provide a versatile tool for controlling sound wave propagation in the design of advanced on-chip integrated acoustic devices, with applications in areas such as acoustic cloaking and sound insulation.

See the supplementary material for details on the effective medium of the segmented waveguide (Fig. S1), the simulated and experimental methods (Fig. S2), and the X- and Y-type evolution of acoustic waves in waveguide arrays (Fig. S3).

This work was supported by the Natural Science Foundation of the Higher Education Institutions of Anhui Province, China (Grant Nos. 2022AH040114, 2022AH050850, and 2023AH051206) and the University Synergy Innovation Program of Anhui Province (Grant No. GXXT-2022-015).

AUTHOR DECLARATIONS

Conflict of Interest

The authors have no conflicts to disclose.

Author Contributions

Ze-Xin Huang: Formal analysis (equal); Investigation (equal); Visualization (equal); Writing – original draft (equal). **Hong-Wei Wu:** Conceptualization (equal); Funding acquisition (equal); Investigation (equal); Project administration (equal); Supervision (equal); Writing – original draft (equal); Writing – review & editing (equal). **Le-Le Cheng:** Investigation (equal); Visualization (equal). **Peng-Xiang Xie:** Investigation (equal); Methodology (equal). **Xue Chen:** Supervision (equal); Validation (equal); Writing – review & editing (equal). **Hua-Feng Xu:** Supervision (equal); Writing – review & editing (equal). **Zong-Qiang Sheng:** Supervision (equal); Validation (equal).

DATA AVAILABILITY

The data that support the findings of this study are available on request from the corresponding author. The data are not publicly available due to state restrictions such as privacy or ethical restrictions.

REFERENCES

[1] S. J. Liang, T. Liu, H. Gao, Z. M. Gu, S. W. An, and J. Zhu, Phys. Rev. Res. **2**, 043362 (2020).
[2] C. Shen, Y. B. Xie, N. Sui, W. Q. Wang, S. A. Cummer, and Y. Jing, Phys. Rev. Lett. **115**, 254301 (2015).
[3] S. Zhang, L. L. Yin, and N. Fang, Phys. Rev. Lett. **102**, 194301 (2009).
[4] D. Lu and Z. Liu, Nat. Commun. **3**, 1205 (2012).
[5] C. Zhang, W. K. Cao, L. T. Wu, J. C. Ke, Y. Jing, T. J. Cui, and Q. Cheng, Appl. Phys. Lett. **118**, 133502 (2021).
[6] H. F. Xie and Z. L. Hou, Phys. Rev. Appl. **15**, 034054 (2021).
[7] Y. B. Xie, W. Q. Wang, H. Y. Chen, A. Konneker, B. Popa, and S. A. Cummer, Nat. Commun. **5**, 5553 (2014).
[8] Y. Li, X. Jiang, R. Q. Li, B. Liang, X. Y. Zou, L. L. Yin, and J. C. Cheng, Phys. Rev. Appl. **2**, 064002 (2014).
[9] Y. Chen and G. K. Hu, Phys. Rev. Appl. **12**, 044046 (2019).
[10] H. W. Wu, Y. Q. Yin, Z. Q. Sheng, Y. Li, D. X. Qi, and R. W. Peng, Phys. Rev. Appl. **15**, 054033 (2021).
[11] Y. Q. Yin, H. W. Wu, S. L. Cheng, W. J. Sun, and Z. Q. Sheng, J. Appl. Phys. **132**, 145101 (2022).
[12] Y. Zhuo, X. Chen, Z. L. Liu, Z. Q. Sheng, and H. W. Wu, Adv. Mater. Technol. **9**, 2301693 (2024).
[13] J. Y. Lu, C. Y. Qiu, L. P. Ye, X. Y. Fan, M. Z. Ke, F. Zhang, and Z. Y. Liu, Nat. Phys. **13**, 369 (2017).
[14] Y. G. Peng, C. Z. Qin, D. G. Zhao, Y. X. Shen, X. Y. Xu, M. Bao, H. Jia, and X. F. Zhu, Nat. Commun. **7**, 13368 (2016).
[15] Z. J. Yang, F. Gao, X. H. Shi, X. Lin, Z. Gao, Y. D. Chong, and B. L. Zhang, Phys. Rev. Lett. **114**, 114301 (2015).
[16] Q. Q. Cheng, Y. M. Pan, H. Q. Wang, C. S. Zhang, D. Yu, A. Gover, H. J. Zhang, T. Li, L. Zhou, and S. N. Zhu, Phys. Rev. Lett. **122**, 173901 (2019).
[17] L. H. Wu and X. Hu, Phys. Rev. Lett. **114**, 223901 (2015).
[18] C. He, X. Ni, H. Ge, X. C. Sun, Y. B. Chen, M. H. Lu, X. P. Liu, and Y. F. Chen, Nat. Phys. **12**, 1124 (2016).
[19] H. Sanchis-Alepuz, Y. A. Kosevich, and J. Sánchez-Dehesa, Phys. Rev. Lett. **98**, 134301 (2007).
[20] N. D. L. Kimura, A. Fainstein, and B. Jusserand, Phys. Rev. B **71**, 041305 (2005).
[21] Z. G. Chen, W. Y. Tang, R. Y. Zhang, Z. X. Chen, and G. C. Ma, Phys. Rev. Lett. **126**, 054301 (2021).
[22] Y. T. Ye, M. Z. Ke, J. H. Feng, M. D. Wang, C. Y. Qiu, and Z. Y. Liu, J. Phys.: Condens. Matter **27**, 155402 (2015).
[23] H. Liu, B. Y. Xie, H. N. Wang, W. W. Liu, Z. C. Li, H. Cheng, J. G. Tian, and Z. Y. Liu, Phys. Rev. B **108**, L161410 (2023).
[24] K. Shandarova, C. E. Rüter, D. Kip, K. G. Makris, D. N. Christodoulides, O. Peleg, and M. Segev, Phys. Rev. Lett. **102**, 123905 (2009).
[25] R. Iwanow, D. A. May-Arrioja, D. N. Christodoulides, G. I. Stegeman, Y. Min, and W. Sohler, Phys. Rev. Lett. **95**, 053902 (2005).
[26] Y. X. Shen, Y. G. Peng, D. G. Zhao, X. C. Chen, J. Zhu, and X. F. Zhu, Phys. Rev. Lett. **122**, 094501 (2019).
[27] Y. X. Shen, L. S. Zeng, Z. G. Geng, D. G. Zhao, Y. G. Peng, and X. F. Zhu, Phys. Rev. Appl. **14**, 014043 (2020).
[28] Y. X. Shen, L. S. Zeng, Z. G. Geng, D. G. Zhao, Y. G. Peng, J. Zhu, and X. F. Zhu, Sci. China Phys., Mech. Astron. **64**, 244302 (2021).
[29] S. Tang, J. L. Wu, C. Lü, J. B. Yao, Y. B. Pei, and Y. Y. Jiang, Appl. Phys. Lett. **122**, 212201 (2023).
[30] S. Tang, J. L. Wu, C. Lü, X. S. Wang, J. Song, and Y. Y. Jiang, Phys. Rev. B **105**, 104107 (2022).
[31] S. Tang, J. L. Wu, C. Lü, J. B. Yao, X. S. Wang, J. Song, and Y. Y. Jiang, New J. Phys. **25**, 033032 (2023).
[32] A. Crespi, F. V. Pepe, P. Facchi, F. Sciarrino, P. Mataloni, H. Nakazato, S. Pascazio, and R. Osellame, Phys. Rev. Lett. **122**, 130401 (2019).
[33] P. W. H. Pinkse, T. Fischer, P. Maunz, and G. Rempe, Nature **404**, 365 (2000).
[34] F. Schäfer, I. Herrera, S. Cherukattil, C. Lovecchio, F. S. Cataliotti, F. Caruso, and A. Smerzi, Nat. Commun. **5**, 3194 (2014).
[35] J. M. Raimond, C. Sayrin, S. Gleyzes, I. Dotsenko, M. Brune, S. Haroche, P. Facchi, and S. Pascazio, Phys. Rev. Lett. **105**, 213601 (2010).
[36] G. Barontini, L. Hohmann, F. Haas, J. Estève, and J. Reichel, Science **349**, 1317 (2015).
[37] A. Signoles, A. Facon, D. Grosso, I. Dotsenko, S. Haroche, J. M. Raimond, M. Brune, and S. Gleyzes, Nat. Phys. **10**, 715 (2014).
[38] R. Morandotti, U. Peschel, J. S. Aitchison, H. S. Eisenberg, and Y. Silberberg, Phys. Rev. Lett. **83**, 2726 (1999).
[39] Q. C. Liu, W. J. Liu, K. Ziegler, and F. Chen, Phys. Rev. Lett. **130**, 103801 (2023).
[40] P. Facchi and S. Pascazio, Phys. Rev. Lett. **89**, 080401 (2002).
[41] P. Facchi, G. Marmo, and S. Pascazio, J. Phys.: Conf. Ser. **196**, 012017 (2009).
[42] P. X. Xie, Z. Q. Sheng, Z. X. Huang, P. Hu, and H. W. Wu, Appl. Phys. Lett. **122**, 222202 (2023).
[43] C. Ma, Y. S. Wang, and J. H. An, Phys. Rev. B **97**, 023808 (2018).
[44] M. A. Nielsen and I. L. Chuang, *Quantum Computation and Quantum Information* (Cambridge University Press, 2000).